On-Chip Hybrid Power Supply System for Wireless Sensor Nodes

WuLong Liu, NICS Lab, E.E. Depart, Tsinghua University
Yu Wang, NICS Lab, E.E. Depart, Tsinghua University
Yuchun Ma, Computer Science Depart, Tsinghua University
Yuan Xie, Computer Science Depart, Pennsylvania State University
Huazhong Yang, NICS Lab, E.E. Depart, Tsinghua University

With the miniaturization of electronic devices, small size but high capacity power supply system appears to be more and more important. A hybrid power source, which consists of a fuel cell (FC) and a rechargeable battery, has the advantages of long lifetime and good load following capabilities. In this paper, we propose the schematic of a hybrid power supply system, that can be integrated on a chip compatible with present CMOS process. For the on-chip fuel cell based hybrid power system in wireless sensor node design, we propose a two steps optimization: 1) dynamic power management (DPM); and 2) adaptive fuel cell optimal power point tracking (AOPPT). The simulation results demonstrate that the on-chip FC-Bat hybrid power system can be used for wireless sensor node under different usage scenarios. Our proposed DPM method can achieve 12.9% energy saving than the situation without DPM method. Meanwhile, implementing our AOPPT approach can save about 17% energy compared with the fixed architecture for the fuel cell system. For an on-chip power system with $1cm^2$ area consumption, the wafer-level battery can power a typical sensor node for only about 5 months, while our on-chip hybrid power system will supply the same sensor node for 2 years steadily.

Categories and Subject Descriptors: B.1 [**Hardware**]: Control Structures and Microprogramming

General Terms: Control, Structures, Microprogramming

Additional Key Words and Phrases: Reconfiguration, On-chip fuel cell, Hybrid power system, Dynamic power management algorithm, Wireless sensor node

1. INTRODUCTION

In recent years, wireless sensor networks (WSN) have gained increasing popularity. For example, wireless sensor networks have a great impact on environment monitoring, data collecting, danger warning, and etc. As we know, power is supplied with the help of energy supply system fitted with the embedded system and is not easily replaceable [Pal et al. 2009; Liu et al. 2012]. For example, regarding the practical WSNs applications for bridge structural health monitoring and animal monitoring, it is costive

and difficult to replace the battery in a short time [Liu et al. 2012]. Thus, energy consumption has become a major challenge for embedded system design. Traditional technologies for solving energy consumption problem mainly focused on two approaches: 1) minimizing the working energy consumption of the embedded system, such as dynamic voltage scale (DVS) [Yuan and Qu 2005] or dynamic frequency scale (DFS) [Yuhua and Longhua 2009]; 2)maximizing the lifetime of the power system [Zhuo and Chakrabarti 2009; Lee et al. 2008; Zhuo et al. 2006]. In this paper, we discuss how to maximize the lifetime of the power system so as to extend the lifetime of wireless sensor nodes (WSN).

In order to maximize the lifetime of power system, several energy self-supply systems have been proposed [Benecke et al. 2009]. These systems could supply themselves depending on converting other energy, such as solar energy, motional energy, chemical energy, and etc, to electronic energy automatically. However, these self-supply systems are not controllable, bulked, and influenced by the environment greatly. Therefore, they are not good choices for the embedded system which needs power supply continuously. In this case, an alternative power supply system must be utilized to keep the embedded system work properly.

As an alternative power source of traditional battery, fuel cell (FC) has attracted much attention. The basic characteristics of a FC are as follows [Zhuo and Chakrabarti 2009].

(1) High Energy Density: In general, compared with Li-ion battery, the fuel cell provides 4 to 10 times energy for the same size and weight.
(2) Environment friendly: Typically, a FC uses hydrogen (H) and oxygen (O) to generate electrical power, and the by-products are water and heat.
(3) Slow and Limited Load Following: Not similar with the traditional batteries, the fuel cells have a narrow load current following range, which is mainly caused by the fact that the slow reaction on the electrode cannot follow quick variation of the load current.

Therefore, fuel cell alone can not meet the power demands of an embedded system with large and frequent current fluctuations. Consequently, one practical solution, hybrid power system (HPS), has been proposed [Zhuo and Chakrabarti 2009; Lee et al. 2008; Zhuo et al. 2006]. The characteristices of different HPSes will be introduced in Section 2. A typical hybrid power system consists of fuel cells worked as the primary source and a rechargeable battery or a supercapacitor worked as the secondary source. In this hybrid power source, the rechargeable battery or the supercapacitor stores surplus energy from the fuel cell during the low demand periods, and provides excessive current during the peak load current demand periods. For the reason that the supercapacitor has lower energy density than the battery, and output voltage of the supercapacitor varies with its charge capacity [Gao 2005], in our work, the hybrid power system is made up of fuel cells and rechargeable battery.

Meanwhile, with the miniaturization of electronic devices, the size has become one of the most important factors in WSN. For example, the size of micro-sensor has decreased to micrometer level. However, the miniaturization of sensor nodes leads to little decrease of energy consumption, sometimes the power increases indeed. One practical way to achieve the high energy capacity and maintain the small size is to integrate one kind of high density power source on one chip or stacked different power sources vertically on one chip. Fruitful work has demonstrated the possibility of on-chip fuel cell [Hahn et al. 2004; Motokawa et al. 2004; Erdler et al. 2006; Yeom et al. 2005; Tominaka et al. 2009; Tominaka et al. 2008; Frank et al. 2009; 2010]and novel rechargeable battery [Notten et al. 2007]. The structure of these on-chip power sources will be presented in Section 3.

From the above discussion, power supply system with small size and high energy density has been one of the most important factors in embedded system design. Based on the current on-chip fuel cell system [Frank et al. 2009; 2010], it is mainly consisted of tens or hundreds of integrated fuel cells. Each cell has the possibility to be broken down or depleted suffering from reliability and unfair usage issues. It is necessary to save power by enhancing the power converting efficiency of fuel cell system and ensure each fuel cell works at the optimal power point with the variation of load profile requirement. Therefore, a robust-aware configuration of fuel cell system is very essential to ensure the power system works properly and efficiently. Besides, an efficient power management algorithm can contribute to further lifetime optimization of the hybrid power supply system. In this paper, we present a robust-aware hybrid power system for wireless sensor nodes design. Our contributions includes:

— We explore the possibility of an on-chip fuel cell based hybrid power system for embedded systems, especially for the wireless sensor nodes design. Since the development of the three-dimensional (3D) integration provides a new chance for integrating different processes on one chip, we also discuss the integration method of the hybrid power system and the sensor circuits.
— We introduce a reconfigurable architecture for on-chip fuel cell system to enhance the robustness of the whole hybrid power system. According to the highly nonlinear current-voltage (I-V) characteristics, an reconfigurable algorithm is proposed to track the optimal power point (OPP).
— We propose a dynamic power management (DPM) algorithm realized by regulating the fuel cell current and the battery charging/discharging state to minimize the energy consumption and extend the lifetime of wireless sensor nodes.
— Our dynamic power management algorithm is extended to suit with different load profiles. And experiments demonstrate the flexibility and efficiency of our dynamic power management algorithm.

The rest of the paper is organized as follows. Section 2 describes the previous work related with our research. Section 3 introduces the schematic of the hybrid power system, the reconfigurable architecture of fuel cells and discusses the possible 3D integration with sensor circuits. We then describe the detailed modeling of this hybrid power system for WSN in Section 4. Section 5 illustrates our dynamic power management algorithm. Section 6 presents the robust-aware reconfiguration algorithm. Section 7 presents the simulation method and discusses the simulation results. Finally, we conclude the paper and present our future work in Section 8.

2. PRELIMINARY OF HYBRID POWER SYSTEMS

2.1. Hybrid Power Systems

In recent years, many hybrid power system structures have been proposed. In general, they can be divided into four categories depending on their components: fuel cell-battery hybrid power system [Zhuo and Chakrabarti 2009; Lee et al. 2008; Zhuo et al. 2006], fuel cell-supercapacitor hybrid power system [Gao 2005; Boulon 2007; Ciancetta 2009; Capponi 2008; Payman 2009; Thomsen 2009], battery- supercapacitor hybrid power system [Shin et al. 2012; Li and G 2008; Zhang and etc 2009; Pay and Baghzouz], and fuel cell-supercapacitor-battery hybrid power system [Ciancetta and etc ; Thounthong and etc ; Thounthong and etc.].

The characters of these hybrid power systems are summarized in Table I. Fuel cell-battery hybrid power system combining the characteristics of fuel cell's high energy density and battery's good load current following ability has been widely used in some portable devices, such as camcorders. With the characteristics of fuel cell's high energy

Table I. Character analysis of four kinds of hybrid power systems

Hybrid Power Systems	FC-Bat Power System	FC-Supercap Power System	Bat-Supercap Power System	FC-Bat-Supercap Power System
Characters	High energy density Good load current following ability Applied in mobile devices	High energy density Large peak current provided Not good short step current provided Applied in Motors	Low energy density Good frequency characteristic Applied in high-power applications	High energy density Good load current following ability High cost of area and complex management Applied in vehicles

density, supercapacitor's high capacity and quick charging or discharging ability, but no transitory step current provided, fuel cell-supercapacitor hybrid power system is always utilized to power some high power devices, such as the vehicles. For battery-supercapacitor hybrid power system, which has relative low energy density comparing with fuel cell-supercapacitor hybrid power system, is always utilized as energy storage system for wind applications or power supply system for some vehicles. Fuel cell-battery -supercapacitor hybrid power system has high energy density, long cycle life, good load current following ability, and etc. However, these advantages are achieved at the cost of large area. In summary, supplying power for some low power devices, especially on-chip devices, such as micro sensor node, **fuel cell-battery hybrid power system is the best choice**.

2.2. On-chip fuel cell and battery integration

In the last few years, fruitful researches have been conducted focused on 2D fuel cell miniaturization and integration so that we can achieve higher power density with smaller footprint [Hahn et al. 2004; Motokawa et al. 2004; Erdler et al. 2006; Yeom et al. 2005; Tominaka et al. 2009; Tominaka et al. 2008; Frank et al. 2009; 2010]. As a representation all of these reported on-chip fuel cells, Frank et al. [Frank et al. 2009; 2010] proposed a new integrated power supply system using on-chip polymer electrolyte membrane (PEM) fuel cells. This power supply system is managed by some CMOS circuits control units, and it can be realized within an extended CMOS process. The detailed fabricated processes and the characteristics of on-chip fuel cells were presented in [Frank et al. 2010]. Besides, Notten et al. [Notten et al. 2007] described a 3D-integrated all-solid-state battery concept, which could prevent electrode degradation upon cycling and electrolyte leakage. In summary, the hybrid power supply system with high energy density and small size can be implemented by the combination of on-chip fuel cell and battery, which will be discussed in detail in the last section.In the paper, we propose the schematic of on-chip fuel cell based hybrid power system which can be compatible with CMOS process.

2.3. Hybrid Power management and the maximum power point tracking method

As we mentioned before, the power management of hybrid power system is critical for the system lifetime. Zhuo et al [Zhuo and Chakrabarti 2009; Lee et al. 2008; Zhuo et al. 2006] proposed dynamic power management algorithm to maximize the lifetime of some "big" embedded systems, such as camcorders. The amount of supplied fuel is controlled by some active system peripheries like pressure reducers and valves. However, for some "small" systems, such as on-chip wireless sensors nodes, the current consumption mainly varies from several uA to several mA which is impossible to achieved by regulating the fuel consumption through some system peripheries. For battery-supercapacitor hybrid power system, constant-current based power management is proposed in [Shin et al. 2012] which is not suitable for the on-chip fuel cell-battery hybrid power system. In this paper, we propose an efficient dynamic power management method for the on-chip wireless sensor node.

In the previous work [Zhuo and Chakrabarti 2009; Lee et al. 2008; Zhuo et al. 2006], the optimal power point is set as an constant for the fuel cell system with a fixed architecture. The maximum power point tracking methods aim to enhance the total output power. Taylor mean value theorem is used to implement a variable step maximum power point tracking method in [Ou et al. 2010]. For the photovoltaic power system, the maximum power point tracking methods are presented based on the exploration of the optimum topology and reconfigurable architecture for solar cells in [Wang et al. ; Xiao et al. 2007] respectively. However, most of the maximum power point tracking methods have high complexity, high energy consumption and large computing resources overhead which do not suit for the low power on-chip wireless sensor node. Besides, the maximum power point but not the maximum power converting efficiency is tracked in the previous work. Thus, the maximum power point may not be the practical optimal power point. In this paper, a simple adaptive optimum power point tracking (AOPPT) method is proposed based on the reconfigurable architecture of the fuel cell system.
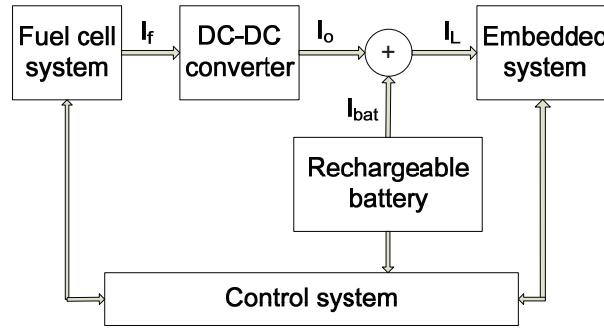
Fig. 1.   The schematic of the hybrid power system for wireless sensor node.

3. HYBRID POWER SYSTEM FOR WIRELESS SENSOR NODE

3.1. The Schematic of Hybrid Power System

The schematic of the hybrid power system is shown in Figure 1. This hybrid power system consists of fuel cell system, rechargeable batteries, DC-DC converter, and control unit. Our proposed optimization method for the hybrid power system mainly consists of two major steps: 1) dynamic power management; 2) adaptive reconfiguration of fuel cell system. For the dynamic power management step, it is to optimize the current and voltage of fuel cell system and rechargeable battery. When the fuel cell current I_f is larger than the load current I_L, external power energy will be used to recharge the battery. Once the battery is full of charge, the external power energy will be bypassed to ground. When the fuel cell current I_f is less than the load current I_L, the rechargeable battery will provide the current difference $I_L - I_o$. For the adaptive reconfiguration of fuel cell system step, it aims at tracking the optimal power point of each fuel cell according to the output current and voltage (I_f, V_f) of the fuel cell system calculated in the first step.

3.2. Components of the Hybrid Power System

3.2.1. on-chip Fuel Cell. Conventional PEM fuel cells consist of a polymer electrolyte membrane (PEM), two gas diffusion electrodes, two diffusion layers, and two flow

fields. The reactants, e.g. hydrogen and oxygen, are supplied to the gas diffusion electrodes over feed pipes out of external tanks. The amount of supplied fuel is often controlled by active system periphery like pressure reducers and valves.
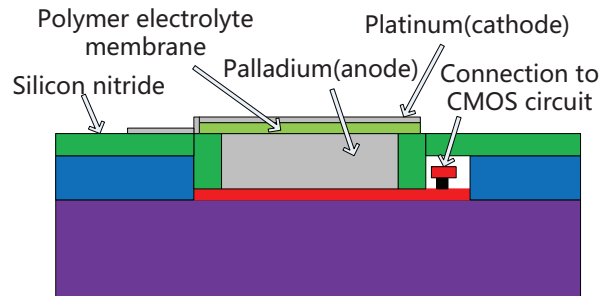
Fig. 2.   Structure of a chip integrated fuel cell.

For a chip integrated PEM fuel cell [Frank et al. 2010], it is made up of a palladium based hydrogen storage and an air breathing cathode both separated by a PEM. Similar with the conventional fuel cell, the FC uses H_2 and O_2 to convert chemical energy to electricity by an electro-chemical process. The hydrogen (H) atoms stored within the palladium are split up into protons and electrons. The electrons flow through the external circuit to the cathode and drive the load. The protons are transported to the cathode through the proton conductive PEM. At the cathode, electrons, protons, and oxygen - supplied by the ambient air - catalytically recombine to water [Frank et al. 2009; Erdler and Frank 2006]. Comparing with conventional FC, chip integration PEM fuel cell does not need external fuel storage and transporting devices. Thus, it can be realized within extended CMOS process. The structure of an integrated fuel cell is illustrated in Figure 2. Actually, the chip integrated fuel cell has the capacity of $500mAh/cm^2$. Compared with state-of-the-art wafer level batteries, $45mAh/cm^2$, the fuel cell has the potential to provide much more capacity [Frank et al. 2010].
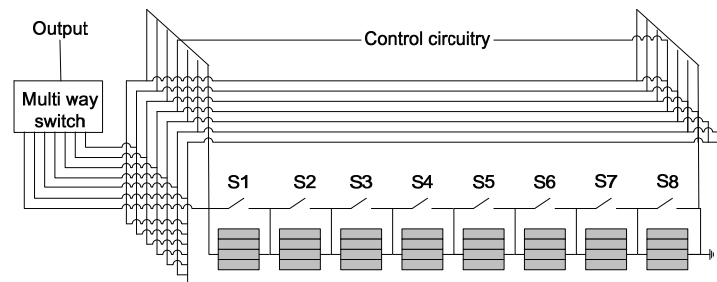
Fig. 3.   On-chip fuel cell cascades connection modeling

3.2.2. Robust-aware and reconfigurable architecture of on-chip fuel cells. In the previous work [Frank et al. 2010; Liu et al. 2011], the connection of the whole on-chip fuel cell system is implemented by the way shown in Figure 3. The system consists of several fuel cell cascades (FCCs) connected in parallel. Each fuel cell cascade is made up of 8 fuel cells, which will provide 3V open voltage. Besides, an external multi-way switch is utilized to control output current of the FCCs by controlling the connected number of FCCs. Although this kind of configuration is robustive and can avoid the broken down or depletion of each fuel cell, the output voltage of each fuel cell cascade is supposed to

be a constant. Once one of these fuel cells in a cascade is broken down, the working state of other fuel cells in the cascade will float away the optimal power point to maintain the constant output voltage. Much more extra fuel will be wasted because of the lower energy converting efficiency. Therefore, an alternative robust-aware and reconfigurable architecture of fuel cell system is very essential to enhance the efficiency and the lifetime of the hybrid power system.
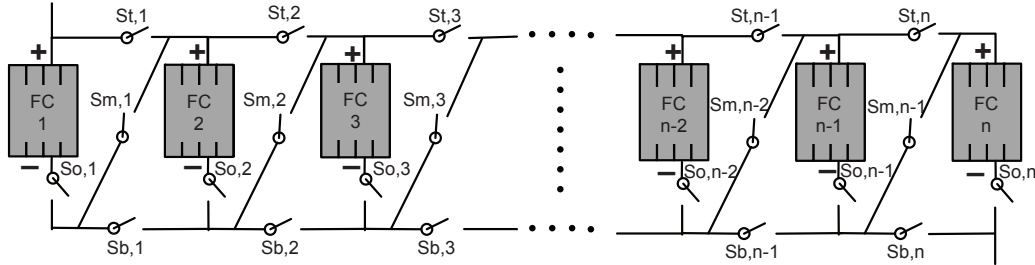
Fig. 4. Reconfigurable architecture with n-FC module
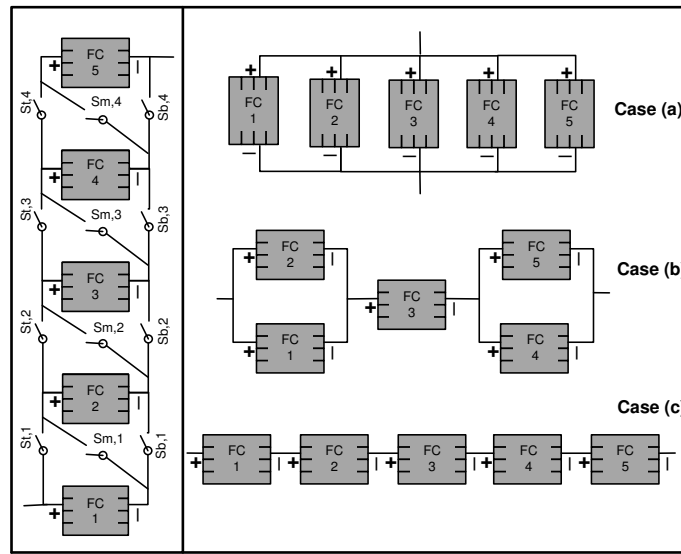
Fig. 5. A reconfiguration example with 5-FC module

The dynamic fuel cell system reconfiguration method is to achieve the optimal output power by regulating the connection configuration of fuel cell system according to the load profile requirement. A reconfigurable fuel cell system structure is shown in Figure 4. It is composed of N fuel cells, and each cell has four switches: St-switches, Sb-switches, Sm-switches, and So-switches. The St-switches and the Sb-switches connect fuel cells in parallel denoted as $S_{t,i}$ and $S_{b,i}$, whereas the Sm-switches connect fuel cells in series denoted as $S_{m,i}$. By controlling the state of each switch, fuel cells can be connected in parallel or series [Wang et al.]. Compared to the reconfigurable architecture proposed in [Wang et al.], we also add one cut-off switch for each fuel

cell denoted as $S_{o,i}$ to turnoff the fuel cell if it is near-depleted or broken down. Figure 5 shows the reconfiguration of a five-cell reconfigurable fuel cell system (N=5 and opten-switches are not shown for simplification). For example, all the St-switches and Sb-switches should be closed and all the Sm-switches should be opened to achieve the configuration in Case (a). For the configuration shown in Case (b), $S_{t,1}$, $S_{b,1}$, $S_{t,4}$, and $S_{b,4}$ are closed, while $S_{m,1}$ and $S_{m,4}$ are opened. $S_{t,2}$, $S_{b,2}$, $S_{t,3}$, and $S_{b,3}$ are opened, while $S_{m,2}$ and $S_{m,3}$ are closed. For the configuration shown in Case (c), all the St-switches and Sb-switches are opened and all the Sm-switches are closed. In addition, the way that dynamic fuel cell reconfiguration can be achieved by the adaptive optimal power point tracking (AOPPT) algorithm according to the required output voltage and current computed by the dynamic power management (DPM) algorithm previously. The detailed DPM and AOPPT algorithms will be presented in Section 5 and 6.

3.2.3. On-Chip Rechargeable Battery. Thin film Si-intercalation electrodes covered with a solid-state electrolyte are found to prevent electrode degradation upon cycling and electrolyte leakage, and has a high energy density appropriately $5mWh/um*cm^2$. Besides, comparing to a super capacitor, the rechargeable batteries have an appropriately constant output voltage. What's more, their energy capacity is more than 3 orders of magnitude higher than that of integrated capacitors. The model of 3D integrated all-solid-state Li-ion battery is shown in Figure 6.
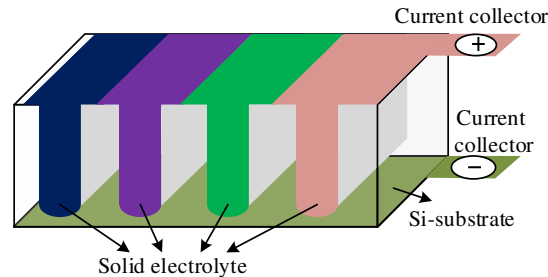
Fig. 6. All solid state Li-ion battery that can be integrated into the 3D hybrid power system [Notten et al. 2007].

3.2.4. Power Control Unit and the Embedded System. In this work, we use the wireless sensor node to act as the embedded system powered by the hybrid power system. Besides, in the whole system, only one processing unit is used, which will handle the data of wireless sensor node and manage the hybrid power system.

3.3. Hybrid Power System Allocation

In order to improve the form factor and consider the cost at the same time, the hybrid power system and sensor circuits can be integrated in one chip or separately allocated on the PCB board. The separated allocation of the power system and sensor circuits will consume larger space with lower cost, while the fully integrated one (e.g. 3D integration with system in a package) will have relatively higher cost but smaller footprint. Here we discuss three different kinds of possible 3D integration cases shown in Figure 7: (a) PCB based 2.5D integration; (b) silicon interposer based 2.5D integration; and (c)Through Silicon Via (TSV) based 3D integration.

3.3.1. PCB based 2.5D integration. Considering the working principle of the fuel cell, the cathode needs to breathe the oxygen from the surrounding air, so we put the fuel cell on the top layer. As shown in Figure 2, first of all, worked as the interconnection
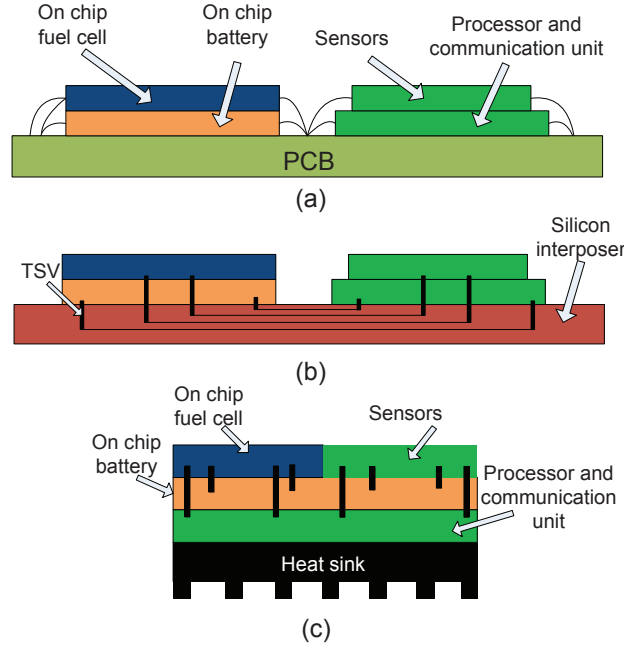
Fig. 7.   Three different structures of the Hybrid Power System for Wireless Sensor Node: (a) PCB based 2.5D integration; (b) silicon interposer based 2.5D integration; and (c) TSV based 3D integration

line, a thin polysilicon film is grown on the p-sub. Then, about 5um palladium related with H atoms is deposited on the polysilicon. Next, 5-10um PEM is deposited by CVD technology. Finally, about 200nm platinum is sputtered on the PEM worked as the anode material [Frank et al. 2010]. To reduce the energy consumption caused by the parasitic effect, the rechargeable batteries will be placed on the second layer.

   The sensor node structure mainly consists of three parts: Data Sensing unit, Processing unit, and Data Communication unit. The date sensing unit is put on the top level, and the processing unit and data communication unit are placed on the bottom level. The communication of different components is through the bonding wire shown in Figure 7(a). This kind of 2.5D integration can achieve relatively smaller footprint but with too many bonding wires on the PCB board.

   3.3.2. Silicon interposer based 2.5D integration. Xilinx has demonstrated the possibility and efficiency of the silicon interposer based 2.5D integration in their Virtex-7 2000T product [Kim et al. 2011]. In this case, if our proposed hybrid power system is integrated on one silicon interposer based 2.5D chip shown in Figure 7(b), it can achieve high bandwidth communication among different components because of the utilization of the TSV in the silicon interposer as an alternative of bonding wires on the PCB board. The stacking order of different components can be similar to the case in PCB based 2.5D integration presented in the last subsection.

   3.3.3. TSV based 3D integration. Except the above two allocation forms of the hybrid power system, the TSV based 3D integration can achieve the smallest footprint and the highest bandwidth between different components as Figure 7(c) shows. However, the shortcoming of this kind of integration is the heat dissipation and the high cost.

Besides, the capacity of the fuel cell system will be limited because both the fuel cell and senors should be placed on the top layer.

According to the above discussion, silicon interposer based 2.5D integration may be the best allocation candidate because it is cost-effective and has high performance.

4. MODELING FOR THE HYBRID POWER SYSTEM

4.1. Fuel Cell Modeling

According to the actual I-V characteristic of the on-chip FCCs [Frank et al. 2009; 2010], it is similar to that of the off-chip fuel cell system which can be divided to three regions [Arsov 2008]: activation region, ohmic region, and concentration region.

4.1.1. Activation Region. A diode can be utilized to simulate the behavior of the activation region: $V_A = Aln(I_f/I_n)$, in which I_n represents the current when I-V characteristic turns from the activation region to ohmic region, I_f is the output current of fuel cells and A is a coefficient.

4.1.2. Ohmic Region. One simple resistance could be used to model the ohmic region: $V_R = RI_f$, in which R is a coefficient.

4.1.3. Concentration Region. A transistor can be used to simulate the concentration region: $V_c = mI_m e^{nI_m I_f}$, in which m, n are coefficients, I_m represents the current when I-V characteristic turns from the ohmic region to concentration region.

The mathematical I-V characteristic of FC is modeled as the following Equation [Arsov 2008]:

$$V = E - A \times ln(I_f/I_n) - R \times I_f - m \times I_m \times e^{nI_m I_f} \tag{1}$$

in which E is the ideal open voltage of FC. Table II and Figure 8 show the fuel cells' model parameters, I-V characteristics and power plot of fuel cells respectively. The detailed characteristics of the fuel cell are shown in Figure 8.

Table II. Parameters used in our FC modeling

Parameters	E (V)	A	I_n (A)	R (Ω)	m	n	I_m (A)
Value	0.375	0.04	0.15	0.0017	0.15	3	0.7

4.1.4. Fuel cell energy converting efficiency. According to Equation 1 and Figure 8, the power loss can also divided into three parts: 1)activation power loss; 2)ohmic power loss; 3)concentration power loss. Then, we can calculate the fuel cell power converting efficiency according to the following Equations.

$$\xi_c = \frac{P_c}{P_{ideal}} \tag{2}$$

$$P_c = V \times I = E \times I - A \times ln(I_f/I_n) \times I - R \times I_f \times I - m \times I_m \times e^{nI_m I_f} \times I \tag{3}$$

$$P_{ideal} = E \times I \tag{4}$$

$$\xi_c = 1 - \frac{A \times ln(I_f/I_n) + R \times I_f + m \times I_m \times e^{nI_m I_f}}{E} \tag{5}$$

in which ξ_c is our defined energy converting efficiency, P_c is the output power of one fuel cell in actual, P_{ideal} is the ideal output power without power loss, and E is the open voltage of one fuel cell. From $I - \xi_c$ characteristic of one fuel cell shown in Figure 8 (C), we can find that the power converting efficiency declines with the increase of the

output current. Besides, we find that the number of utilized fuel cells has a great relationship with the output power of each fuel cell. When the fuel cell works at the lower power point, there will be much more fuel cells utilized, which tends to be unstable. In order to make a tradeoff between the power converting efficiency and the number of fuel cells utilized, in this work, the optimal output power point of one fuel cell is set as the 2/3 of the maximum power point(0.19mA, 0.2087V) marked in Figure 8. Besides, this power point can guarantee the convergence of our AOPPT algorithm with the limitation of less than 300 fuel cells for the load profile in our experiment. Our AOPPT algorithm presented in Section 6 will attempt to track this optimal power point for each fuel cell.
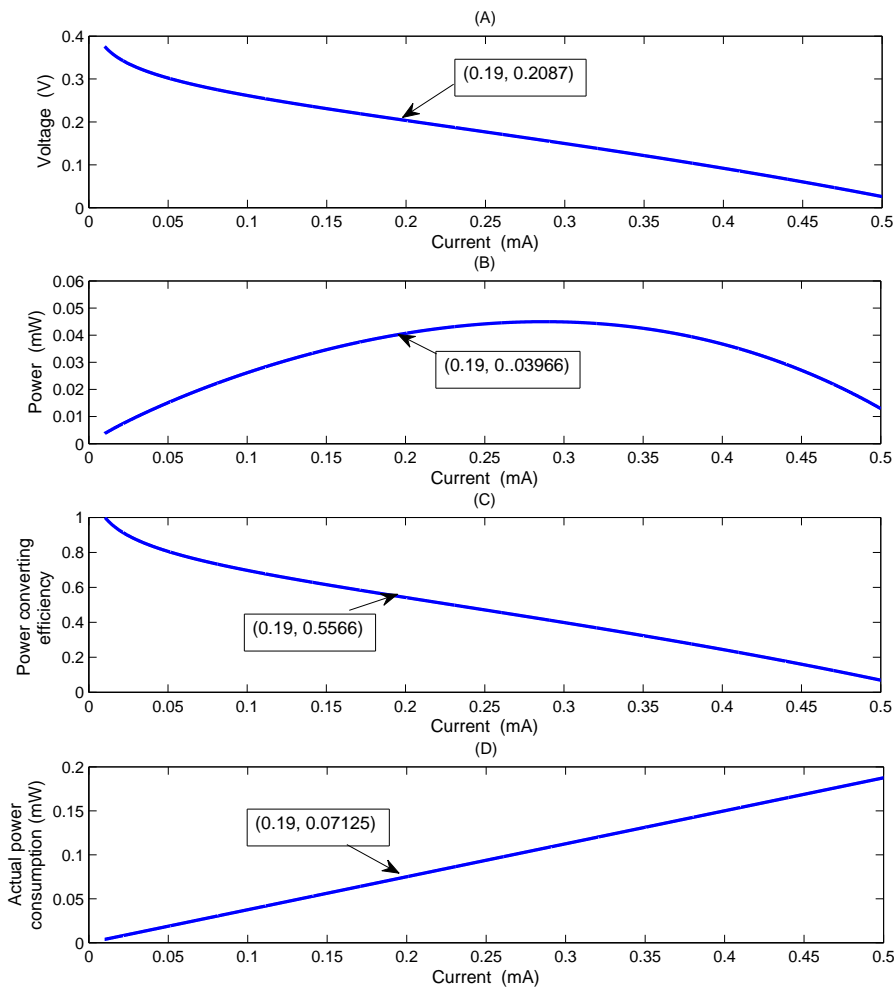
Fig. 8.   The characteristics of one fuel cell: (A)the output current-voltage polarization; (B)the output current-power polarization; (C)the output current-power converting efficiency plot of one fuel cell; and (D)the output current-the actual power consumption of one fuel cell. The optimal working point is also marked.

4.2. Rechargeable Battery Modeling

According to the measured data presented in [Notten et al. 2007], the model of on-chip battery is similar to the characteristic of traditional Li-ion rechargeable batteries as the following expressions.

$$V = \begin{matrix} 0.5 * SOC + 0.8, 0 < SOC \le 0.2 \\ 0.25 * SOC + 0.85, 0.2 \le SOC < 1 \end{matrix} \tag{6}$$

and

$$SOC = (\int_0^t (I_o - I_l) dt)/C_{max} \tag{7}$$

where SOC is the state of charge, I_l is the load current, I_o is the output current, C_{max} is is the maximum capacity of rechargeable battery. Actually, the electrical-to-chemical power converting efficiency of the battery varies with its service time. In this work, we suppose both of the discharging and charging energy converting efficiency, ϕ_{disch}, ϕ_{ch} as a constant just for simplification.

4.3. DC-DC Converter Modeling

Since the output voltage of fuel cell and rechargeable battery tends to be a constant, we define the DC-DC converting efficiency using a linear model [Lee et al. 2008] as $\eta = \alpha - \beta I_o$, where α, β are the empirical value decided by the actual converting efficiency.

5. DYNAMIC POWER MANAGEMENT ALGORITHM

Table III. Definitions in our dynamic power management algorithm for WSN

C_{max}	The maximum charge capacity of the battery
I_{max}	The maximum output current of the fuel cell
I_{min}	The minimum output current of the fuel cell
$Q_{ini}(k)$	The charge state of the battery at the initial of Kth task
$Q_{end}(k)$	The charge state of the battery at the end of Kth task
$I_{o|s}(k)$	The output current of the DC-DC converter at the Sleep state
$I_{o|A}(k)$	The output current of the DC-DC converter at the Active state
$I_{l|S}(k)$	The load current at the Sleep state
$I_{l|lis}(k)$	The load current at the Listening state
$I_{l|C}(k)$	The load current at the Communication state
$T_S(k)$	The Sleep state time
$T_I(k)$	The Idle state time
$T_{lis}(k)$	The Listening state time
$T_C(k)$	The Communication state time
I_{fc}	The output current of the fuel cell system
V_{fc}	The output voltage of the fuel cell system
P_c	The output power of one fuel cell
P_{fc}	The output power of the fuel cell system
μ_{sp}	The permitted maximum idle time
μ_a	The permitted time to regulate the fuel cell current in Active period

Based on the dynamic power management algorithm on hybrid power system [Lee et al. 2008], we propose a hybrid power system optimization method for wireless sensor node with different working modes. In general, the wireless sensor node has four states: *Sleep*, *Idle*, *Listening*, and *Communication*. Firstly, once $T_I(k) > \mu_{sp}$, the power system will be put into *Sleep* state. We consolidate the *Listening* and *Communication* states as Active state. Then, in the *Sleep* state, the battery will be charged. In the *Active* state, the battery will be discharged to provide the external load current. As we

know, the *Communication* state needs a large current and the battery has a well load current following ability. Thus, when the fuel cell current tends to be constant during the *Active* state, the battery could provide this peak current rapidly. The outline of our modified dynamic power management algorithm is shown in Figure 9.

We begin with some definitions used in this algorithm as shown in Table III. Our goal is to minimize the fuel consumption for each task. We assume that $I_{o|A}(k)$, $I_{o|s}(k)$ are constants during the k-th task slot. $T_s(k)$, $T_{lis}(k)$, $T_C(k)$ could be obtained from the load profile before we perform the task. Besides, according to the DC-DC converting efficiency,

$$I_{fc} = (V_o \times I_o)/(\xi \times \eta) \approx (0.3 \times I_o)/(\alpha - \beta I_o) \tag{8}$$

where V_o is the output voltage of DC-DC converter, and ξ is the power efficiency of fuel cell defined in Section 4.1.4.

Hence, the fuel consumption is given by

$$\begin{aligned}
C(k) &= (0.3 \times I_{o|s}(k)) \times T_S/(\alpha - \beta I_{o|s}(k)) + \\
&\quad (0.3 \times I_{o|A}(k) \times (T_{lis}(k) + T_C(k)))/(\alpha - \beta I_{o|A}(k))
\end{aligned} \tag{9}$$

Then taking the battery state for consideration, in each k-th task slot, we consider the case when $Q_{ini}(k) \neq Q_{end}(k)$. Since $Q_{ini}(k) = Q_{end}(k-1)$, $Q_{ini}(k)$ is a known value. We suppose that $Q_{end}(k) = Q_{ini}(1)$ for each round optimization. According to the rule of conservation of charge, we give out the following expression.

$$\frac{Q_{ini}(k) + (I_{o|s}(k) - I_{l|s}(k)) \times T_s(k)}{\phi_{ch}} = \tag{10}$$
$$\frac{(I_{o|lis}(k) - I_{o|A}(k)) \times T_{lis}(k) + (I_{o|c}(k) - I_{o|A}(k)) \times T_C(k)}{\phi_{disch}}$$

Besides, in each cycle, we define that the ending discharge state pluses the discharging capacity should be less than the maximum capacity of the battery, which can be indicated by the following expression.

$$Q_{end}(k) + \frac{(I_{l|lis}(k) - I_{o|A}(k)) \times T_{lis}(k)}{\phi_{disch}} + \frac{(I_{l|c}(k) - I_{o|A}(k)) \times T_C(k)}{\phi_{disch}} \leq C_{max} \tag{11}$$

Then, because of the narrow load current range of the fuel cells, we define the limitation that

$$I_o \in [0.01, 1] \tag{12}$$

Thus, when Equation (9) is taken as the **objective function** and Equations (10), (11), (12) as the **constraints**, we can find out the optimal value of $I_{o|s}(k)$ and $I_{o|A}(k)$. At last, the output current of fuel cell I_{fc} during *Active* and *Sleep* modes can be decided by Equation (8).

We also consider two extreme operation cases. First, if active time $T_a = T_{lis}(k) + T_C(k) \leq \mu_a$ in one task, that means the active time is too short, we will keep the output current of the fuel cell as constant: $I_{o|s}(k) = I_{o|A}(k) = I_o(k)$. In the other case, if active time or communication time $T_C(k)$ in one task lasts too long and cannot meet constraints in Equations (10) and (11). We define that both the initial charge of battery in k-th task and the charging capacity during *Sleep* period equal to the discharging

capacity in listening period which can be expressed in Equation (13). While during the *Communication* state, all the current demand will be only provided by regulating the multi ways switch in FCCs, which means to increase the output current of FCCs, although the FCCs' efficiency will be lower. Therefore Equation (13) will take place of Equation (10) as a constraint.

$$Q_{ini}(k) + \frac{(I_{o|s}(k) - I_{l|s}(k)) \times T_s(k)}{\phi_{ch}} = Q_{end}(k) + \frac{(I_{l|lis}(k) - I_{o|A}(k)) \times T_{lis}(k)}{\phi_{disch}} \quad (13)$$
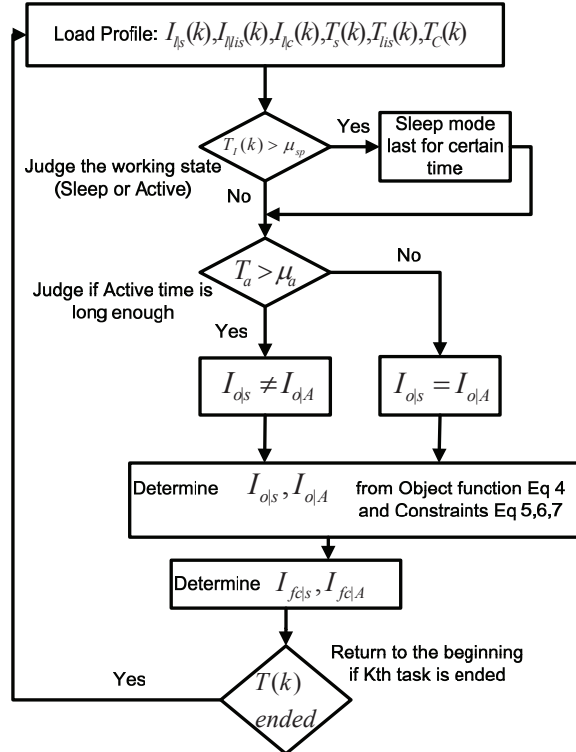
Fig. 9.   Our modified DFM algorithm for WSN.

Note that the computation complexity of our proposed DPM algorithm depends on the pre-defined computation error ε, which is the absolute difference value between the computed value and the actual optimal value. The computation error ε has a inverse proportion with the simulation step for each iteration, which also means that the computation time has a direct proportion with the pre-defined computation error ε. Our experimental results show that the computation time of our proposed DPM algorithm is only tens of ms when the convergence error is 2%.

6. ADAPTIVE OPTIMAL POWER POINT TRACKING ALGORITHM FOR FUEL CELL SYSTEM

Based on the reconfiguration architecture shown in Section 3.2.2, we propose a simplified adaptive optimal power point tracking (AOPPT) algorithm for the fuel cell system. Once the optimum output voltage and current of the fuel cell system are determined by the previous DPM method, our AOPPT algorithm can achieve a kind of fuel cells' configuration that ensures all the fuel cells work at or near their optimal output power

Table IV. Definitions in our AOPPT algorithm for fuel cell system

N	The total number of fuel cells
N_{update}	The number of available fuel cells
V_{co}	The opten-voltage of the fuel cell
V_{cd}	The depleted-voltage of the fuel cell
V_c	The optimum output voltage of the fuel cell
I_c	The optimum output current of the fuel cell
n_{s_opt}	The original optimum number of fuel cell modules connected in series
n_{p_opt}	The original optimum number of fuel cell modules connected in parallel
n_s	The final optimum number of fuel cell module connected in series
n_p	The final optimum number of fuel cell module connected in sparallel
$S_{o,i}$	The state of opten-switch for the i-th fuel cell

point. Figure 10 shows the pseudo-code of our proposed AOPPT algorithm. When the output current and voltage of fuel cell system optimized by DPM algorithm is obtained, the state of charge (SoC) is checked for all the fuel cells at first. In general, SoC of the fuel cell is the linear function of the voltage. Therefor, we utilize the voltage difference to evaluate the charge state of the fuel cell as shown in Equation (10). ρ is the ratio to judge whether one fuel cell is near-depleted. The fuel cell will be turned off when its charge state is lower than the boundary. In this way, all the available fuel cells are checked and the number of available fuel cells N_{update} is updated.

$$V_c - V_{cd} \leq \rho(V_{co} - V_{cd}) \tag{14}$$

The next stage is to calculate the original optimum numbers of fuel cell modules connected in series and parallel. All the fuel cells are supposed as working at their optimal power point(V_{c_opt},I_{c_opt}). The original optimum numbers of fuel cell modules connected in series and parallel equals to round-off numbers shown in Equation (11).

$$n_{s\_opt} = [\frac{V_{fc}}{V_{c\_opt}}]; \quad n_{p\_opt} = [\frac{I_{fc}}{I_{c\_opt}}] \tag{15}$$

Then, a step of regulating procedure is implemented to further optimize the configuration of the fuel cell system. When $n_{s\_opt} \times n_{p\_opt}$ is equal to or smaller than the number of available fuel cells N_{update}, it means that it is unnecessary to make all the available fuel cells work at their optimal power point (V_{c_opt},I_{c_opt}). In other words, some fuel cells with the fewest SoC can be turned off to save power. All the available fuel cells are sorted according to their SoC values and the last $N_{update} - n_{s\_opt} \times n_{p\_opt}$ fuel cells with the fewest SoC are turned off. The final optimum numbers of fuel cell modules connected in series and parallel (n_s and n_p) equal to the original optimum values n_{s_opt} and n_{p_opt}.

For the situation that $n_{s\_opt} \times n_{p\_opt}$ is larger than the number of available fuel cells N_{update}, it means that all the available fuel cells are not sufficient to output the required voltage and current (V_{fc}, I_{fc}) if each fuel cell works at its optimal power point. In order to achieve a balanced configuration of the fuel cell system and meet the requirement of load profile, all the fuel cells should float away their optimal power point (V_{c_opt},I_{c_opt}). In this work, our reconfiguration algorithm tries to achieve the minimum power consumption and track the optimal power point of each fuel cell. Therefore, the optimization problem can be summarized as the following Equations. **Minimize:**

$$f(V_c, I_c) = \mu \times \frac{n_s \times n_p \times V_c \times I_c}{\xi_c} + \nu \times (|I_c - I_{c\_opt}| \tag{16}$$

Subject to the following Equations (13)-(14) and Equation (1):

$$n_s = [\frac{V_{fc}}{V_c}]; \quad n_p = [\frac{I_{fc}}{I_c}] \tag{17}$$

$$n_s \times n_p \leq N_{update} \tag{18}$$
$$|(n_s \times V_c) - V_{fc}| \leq \lambda V_{fc} \tag{19}$$

in which μ, ν are the weights to make a tradeoff between the power consumption and the deviation from the optimal power point. In this work, we set the value of μ, ν as 0.6 and 0.4 respectively. Besides, the actual output voltage of the fuel cell system $(n_s \times V_c)$ should not deviate from the ideal required output voltage V_{fc} in a certain percent, defined in Formula (19). In this work, the value of λ is set as 30%.

Note that the extra power switches shown in Figure 4 are the main hardware overhead, which only take a small part of the whole power system. The computation overhead also mainly depends on the convergence error as discussed in Section 5.

The AOPPT Algorithm

Input: output current and voltage of fuel cell system optimized by DPM algorithm: I_f, V_f

For each FC i=1 to N:

  $S_{o,i} \longleftarrow$ Check_SoC(i);

  update N;

End

Calculte the original n_{s_opt}, n_{p_opt} values using Equation (15);

If $n_{s\_opt} \times n_{p\_opt} \leq N_{update}$

  Sort all fuel cells according to their SoC value;

  For all the last $N_{update} - n_{s\_opt} \times n_{p\_opt}$ fuel cells with the fewest SoC

    i=1 to $(N_{update} - n_{s\_opt} \times n_{p\_opt})$:

    $S_{o,i} = 0$;

  End

  $n_s = n_{s\_opt}$; $n_p = n_{p\_opt}$;

  Return n_s, n_p and all open-switches states S_o

Else

  Find the optimum working state for each fuel cell (I_c, V_c) using Equation (16)-(18);

  Calculate n_s, n_p using Equation (15)

Return n_s, n_p

Fig. 10.   Pseudo-code of our proposed adaptive maximum power point tracking algorithm for fuel cell system

7. CASE STUDY

7.1. Experimental setup

A typical wireless sensor node applied in low duty cycle is utilized in our work, which mainly consists of Micaz and MTS310 [Kramer and Geraldy 2006], and has a 7.3728MHZ working frequency, 250 kbps transferring rate. Two types of data, Light

and Temperature information, are acquired in each cycle (the cycle time is 70 seconds). This acquired information could be transferred in its cycle or accumulated into another cycle to be transferred together. In Figure 12, the current consumption within one working cycle is presented and scaling to on-chip integrated conditions. Figure 11 shows the simulator in Matlab/Simulink used in our experiment. In this work, from the point of minimized energy consumption, we will evaluate how the hybrid power system behaves and then find out the most efficient operating pattern.
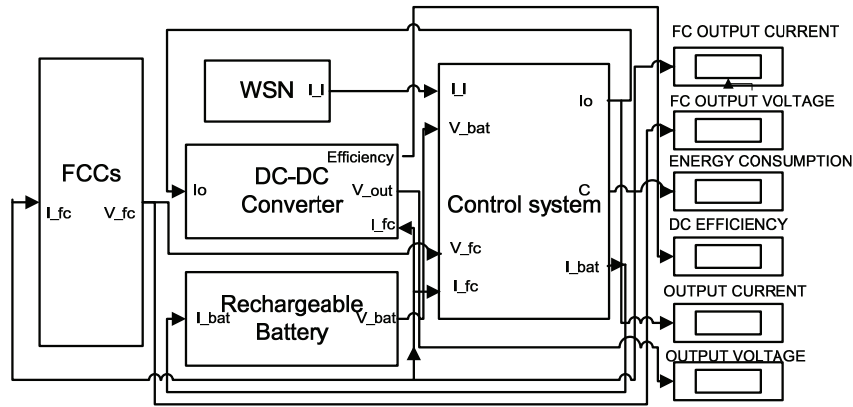
Fig. 11.   FC-Bat hybrid system simulator in Matlab/simulink.
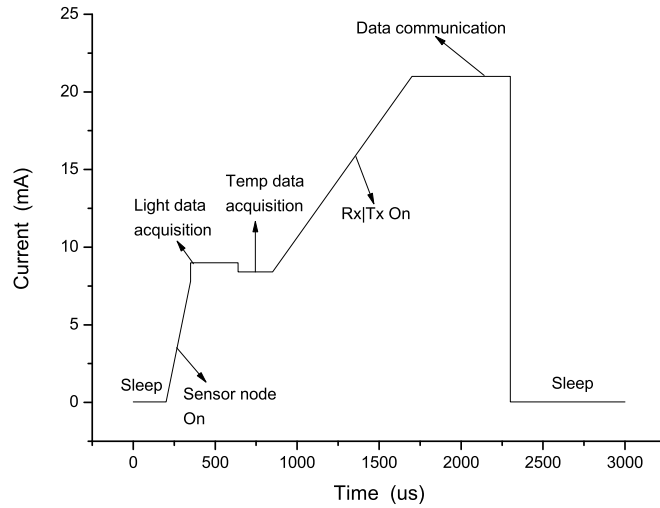
Fig. 12.   A typical current load profile of a wireless sensor node. [Kramer and Geraldy 2006]

7.2. The superiority of our on-chip hybrid power system with DPM method than the wafer-level battery

In this work, we compare this on-chip FC-Bat hybrid power system with traditional wafer-level battery as shown in Table V. When the chip area is assumed as $1cm^2$ and the whole power system has two layers, the wafer-level battery's capacity is about 45*2=90mAh, while on-chip FC-Bat hybrid power system's capacity is 500mAh [Frank et al. 2010]. The simulation results demonstrate that the wafer-level battery can power a typical sensor node for only about 5 months, while our on-chip hybrid power system could supply a typical sensor node for over 2 years steadily. Besides, when fuel cell system and rechargeable battery are just parallel connected without dynamic power management, it has more than 12.9% energy consumption than utilizing our DPM method.

Table V. Comparisons of two kinds of power sources: wafer-level battery and our proposed hybrid power system with/without DPM method. EC: Energy Consumption

Power Source	Chip Area cm^2	Capacity (mAh)	EC per cycle (mJ)	Life time (year)
Wafer-level battery [Song and et al. 2009]	1	45*2	1.9208	0.374
Hybrid power system without DPM	1	500	1.823	2.227
Hybrid power system with DPM	1	500	1.614	2.475
Extension ratio without DPM	1.0	5.56	0.949	5.955
Extension ratio with DPM	1.0	5.56	0.840	6.618

Table VI. Energy Consumption (EC) of five working patterns (mJ)

Operation modes: Communication within	Total EC	Average EC per cycle	EC with battery only
one cycle	1.6140	1.6140	1.9208
two cycles	3.214	1.6070	3.8292
three cycles	4.8152	1.6051	5.7375
four cycles	6.4173	1.6043	7.6459
five cycles	8.0184	1.6037	9.5542

7.3. Analysis with different load profiles

By regulating sensor node's operated cycle numbers of data acquisition, we obtain the total and average energy consumption in five operation modes as shown in Table VI. Comparing with the situation that powered with only wafer-level battery, our proposed DPM algorithm on FC-Battery hybrid power system can save 16% more energy. From Figure 12, the sensor node gets light and temperature data in each cycle, but we can save them and transfer the data at one time. From Table VI, we conclude that the more acquisition data stored to be transferred in one cycle, the less energy will be consumed by one sensor node per cycle. However, from the curve of average energy consumption per cycle with five operation modes showed in Table VI, we find that the average energy consumption per cycle will reduce little after the communication period is greater than 4 cycles. Meanwhile, the stored acquisition data numbers are directly proportional to the efficiency of data storage and processing. Comprehensively considered, the operation mode with four acquisition cycles and data transferred in the fourth cycles will be the most efficient operation mode in our scenario.

Figure 14 gives the detailed FCCs output current I_o during data communication cycle in six operation modes (transferring 0-6 data packages). We can see from the current profile, I_o variation located among the region of $[0, 1mA]$. Because larger variation of I_{fc} between active and sleep states results in larger fuel consumption, the

output current under DPM algorithm is much more flatter and results in lower fuel consumption according to Equation (3).

We keep all the conditions the same of a typical data transferred within one cycle but regulating the Sleep state's time. This corresponds to the curve shown in Figure 13. The results show that energy consumption in one operation cycle increases in linear relation with the cycle time. Besides, holding the cycle time as 70s, when we change the communication/active time, the relation of active time, energy consumption, and transferred data is shown in Figure 15, which demonstrates that energy consumption in data communication cycle is proportional to the amount of communicated data.
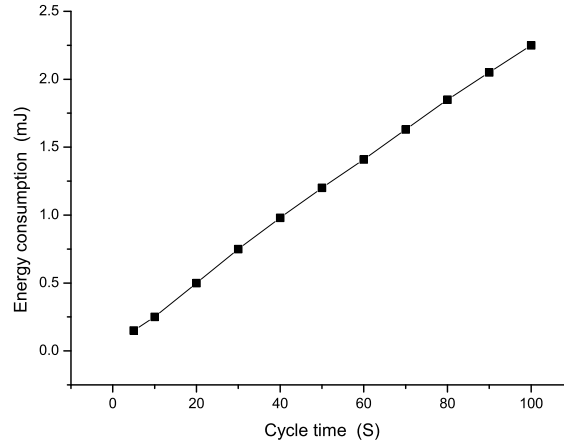
Fig. 13.   Energy consumption per cycle varies with the cycle time.

Then, we discuss one case that one task is accomplished in a 70s working cycle and another case that one task is accomplished within five subtasks which has a 14s cycle time. The simulation results in Table VII show that one task accomplished within five cycles has less energy consumption than one task accomplished in one cycle.

Finally, we consider two extreme working states of sensor node as shown in Table VIII. The simulation results demonstrate that when the sensor node works at the extreme states, FC-Bat hybrid power system also has less energy consumption than the one powered with battery only.

Table VII. Simulation results in one whole task or five sub-tasks. I_{o-a} and I_{o-i} are the output current for active state and idle state

Operation mode	I_{o-a} (mA)	I_{o-i} (mA)	Battery capacity (mAs)	Energy Consumption (mJ)
One Task	0.996	0.03646	0.70	2.6470
Five subtasks	0.998	0.03623	0.14	2.6145

Table VIII. Simulation results of two extreme operation states.

Operation state	Active time (mS)	Cycle time (S)	Hybrid EC (mJ)	Battery only EC (mJ)
Long active state	100	70	3.6857	4.0016
Short active state	1	70	1.588	1.9043
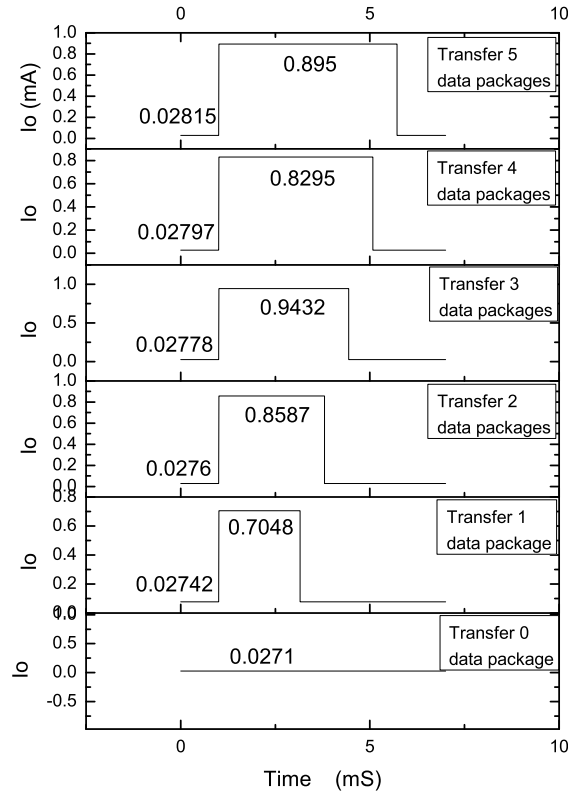
Fig. 14.   Output Current of fuel cell within one transferring cycle in six working states.

Table IX. Comparisons of two architectures for fuel cell system: fixed architecture [Liu et al. 2011] and reconfigurable architecture. EC: energy consumption; n_s, n_p: the series and parallel connected number of fuel cells; I_{fc}, V_{fc}: the actual output current and voltage of the fuel cell system utilizing AOPPT. Case1 to Case6 refer to the six working states that sampling data is not transferred or accumulated to be transferred in 1 to 5 cycles.

Cases	Sleep State				Active State				EC Consumption		EC Reduction
	I_{fc_s}	V_{fc_s}	n_{s_s}	n_{p_s}	I_{fc_a}	V_{fc_a}	n_{s_a}	n_{p_a}	Fixed Arch	AOPPT	Ratio
Case1	0.0167	1.0620	3	1	0.0167	1.0620	3	1	1.6010	1.3160	17.79%
Case2	0.0169	1.0605	3	1	1.4322	1.0045	5	7	1.6140	1.3354	17.26%
Case3	0.0170	1.0599	3	1	3.6708	0.7375	5	12	3.2140	2.6514	17.50%
Case4	0.0171	1.0590	3	1	9.8736	1.0500	7	33	4.8152	4.0303	16.30%
Case5	0.0173	1.0575	3	1	2.9190	1.0310	5	15	6.4173	5.3212	17.08%
Case6	0.0174	1.0566	3	1	5.1140	1.0416	6	20	8.0184	6.6573	16.97%

7.4. Comparison the results with or without our AOPPT algorithm

As Section 3.2.2 and Section 6 state, we propose a reconfigurable architecture and an adaptive optimal power point tracking (AOPPT) algorithm for the fuel cell system. In order to demonstrate the superiority of our proposed architecture and algorithm, we compare our reconfigurable architecture with the fixed architecture shown in Figure 3. As Figure 14 shows, we explore six different working states of the WSN, which accumulate the sampling data to be transferred in different cycles. By implementing our proposed AOPPT method for these six kinds of working states of the WSN, we can
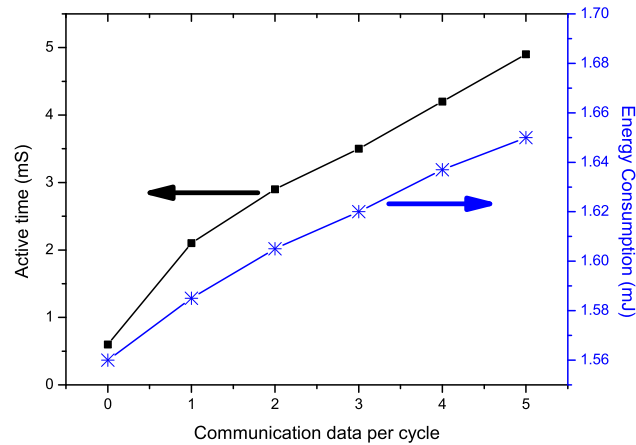
Fig. 15.   Active time and energy consumption under six communication modes.

achieve about 17% energy reduction compared with the fixed architecture shown in Table IX.

8. CONCLUSIONS

In this paper, we proposed the schematic of fuel cell based on-chip FC-Bat hybrid power system which consists of on-chip fuel cells served as the primary source and on-chip rechargeable battery served as the secondary source. Then, we addressed the problem of maximizing the lifetime of a fuel-cell based hybrid power system. We proposed a two-step optimization method, dynamic power management and adaptive optimal power point tracking algorithm, for on-chip FC-Bat hybrid power system used in WSN. Taking the wireless sensor node powered by this hybrid power system as an example, the simulation results demonstrated our proposed DPM method can achieve 12.9% energy saving than the situation without DPM method. Meanwhile, implementing our AOPPT approach can save about 17% energy compared with the fixed architecture for the fuel cell system. For one on-chip power system with $1cm^2$ area, the wafer-level battery can power a typical sensor node for only about 5 months, while our on-chip hybrid power system can supply the same sensor node for over 2 years steadily.

REFERENCES

ARSOV, G. L. 2008. Improved parametric pspice model of a pem fuel cell. *IEEE OPTIM 2008. 11th. Conference*, 203–208.

BENECKE, S., NISSEN, N., AND REICHL, H. 2009. Environmental comparison of energy scavenging technologies for self-sufficient micro system applications. *IEEE on ISSST*, 1–6.

BOULON, L. P. 2007. Energetic macroscopic representation of a fuel cell-supercapacitor system. *IEEE VPPC*, 290–297.

CAPPONI, B. V. 2008. A fuel cell-supercapacitor power supply for portable applications. *COMPEL*, 1–4.

CIANCETTA, F. AND ETC. The modeling of a pem fuel cell-supercapacitor-battery system in dynamic conditions. *PTC. 2009. IEEE*, 1–5.

CIANCETTA, F. B. 2009. System pem fuel cell-supercapacitor: Analysis in transitory conditions. *ICCEP*, 154–158.

ERDLER, G. AND FRANK, M. 2006. Chip integrated fuel cell. *19th European Conference on Solid-State Transducers 132*, 331–336.

ERDLER, G., FRANK, M., LEHMANN, M., REINECKE, H., AND MLLER, C. 2006. Chip integrated fuel cell. *Sensors and Actuators A: Physical 132,* 1, 331 – 336. ¡ce:title¿The 19th European Conference on Solid-State Transducers¡/ce:title¿.

FRANK, M., KUHL, M., ERDLER, G., AND FREUND, I. 2009. An integrated power supply system for low-power 3.3v electronics using on-chip polymer electrolyte membrane (pem) fuel cells. *ISSCC Dig. Tech.*, 292–293.

FRANK, M., KUHL, M., ERDLER, G., AND FREUND, I. 2010. An integrated power supply system for low-power 3.3v electronics using on-chip polymer electrolyte membrane (pem) fuel cells. *IEEE Journal of Solid-State Circuits 45*, 205–213.

GAO, W. May 2005. Performance comparison of a fuel cell-battery hybrid powertrain and a fuel cell-ultracapacitor hybrid powertrain. *IEEE Trans. Vehicular Technology 5*, 846–855.

HAHN, R., WAGNER, S., SCHMITZ, A., AND REICHL, H. 2004. Development of a planar micro fuel cell with thin film and micro patterning technologies. *Journal of Power Sources 131,* 1C2, 73 – 78. ¡ce:title¿Selected papers presented at the Eighth Grove Fuel Cell Symposium¡/ce:title¿.

KIM, N., WU, D., KIM, D., RAHMAN, A., AND WU, P. 2011. Interposer design optimization for high frequency signal transmission in passive and active interposer using through silicon via (tsv). In *Electronic Components and Technology Conference (ECTC), 2011 IEEE 61st*. 1160 –1167.

KRAMER, M. AND GERALDY, A. 2006. Energy measurements for micaz node. *Technical Report*.

LEE, K., CHANG, N., AND ZHUO, J. 2008. A fuel-cell-battery hybrid for portable embedded systems. *ACM Trans on Computational Logic 1*, 1–34.

LI, W. AND G, J. 2008. A power electronic interface for a battery supercapacitor hybrid energy storage system for wind applications. *PESC, IEEE*, 1762–1768.

LIU, W., FEI, X., TANG, T., WANG, P., LUO, H., DENG, B., AND YANG, H. 2012. Application specific sensor node architecture optimization —experiences from field deployments. In *Design Automation Conference (ASP-DAC), 2012 17th Asia and South Pacific*. 389 –394.

LIU, W., WANG, Y., LIU, W., MA, Y., XIE, Y., AND YANG, H. 2011. On-chip hybrid power supply system for wireless sensor nodes. In *Design Automation Conference (ASP-DAC), 2011 16th Asia and South Pacific*. IEEE, 43–48.

MOTOKAWA, S., MOHAMEDI, M., MOMMA, T., SHOJI, S., AND OSAKA, T. 2004. Mems-based design and fabrication of a new concept micro direct methanol fuel cell (-dmfc). *Electrochemistry Communications 6,* 6, 562 – 565.

NOTTEN, P. H., ROOZEBOOM, F., AND NIESSEN, R. A. 2007. 3-d integrated all-solid-state rechargeable batteries. *Adv. Mater 19*, 4564C4567.

OU, Y., WANG, C., AND HONG, F. 2010. A variable step maximum power point tracking method using taylor mean value theorem. In *Power and Energy Engineering Conference (APPEEC), 2010 Asia-Pacific*. 1 –4.

PAL, Y., AWASTHI, L., AND SINGH, A. 2009. Maximize the lifetime of object tracking sensor network with node-to-node activation scheme. *IEEE on IACC*, 1200–1205.

PAY, S. AND BAGHZOUZ, Y. Effectiveness of battery- supercapacitor combination in electric vehicles. *PTC 2003, IEEE 3*.

PAYMAN, A. P. 2009. Flatness based control of a fuel cell-supercapacitor multi source/multi load hybrid system. *EPE 09. 13th European conf. Power Electronics and Applications*, 1–10.

SHIN, D., KIM, Y., WANG, Y., CHANG, N., AND PEDRAM, M. 2012. Constant-current regulator-based battery-supercapacitor hybrid architecture for high-rate pulsed load applications. *Journal of Power Sources 205*, 516–524.

SONG, J. AND ET AL. 2009. Solid-state microscale lithium batteries prepared with microfabrication processes. *J. Micromech. Microeng 19*.

THOMSEN, Z. Z. 2009. A two-stage dc-dc converter for the fuel cell-supercapacitor hybrid system. *ECCE*, 1425–1431.

THOUNTHONG, P. AND ETC. Control of fuel cell/battery/ supercapacitor hybrid source for vehicle applications. *ICIT. 2009. IEEE*, 1–6.

THOUNTHONG, P. AND ETC. Performance evaluation of fuel cell/battery/supercapacitor hybrid power source for vehicle applications. *IAS. 2009. IEEE*, 1–8.

TOMINAKA, S., NISHIZEKO, H., MIZUNO, J., AND OSAKA, T. 2009. Bendable fuel cells: on-chip fuel cell on a flexible polymer substrate. *Energy Environ. Sci. 2*, 1074–1077.

TOMINAKA, S., OHTA, S., OBATA, H., MOMMA, T., AND OSAKA, T. 2008. On-chip fuel cell: Micro direct methanol fuel cell of an air-breathing, membraneless, and monolithic design. *Journal of the American Chemical Society 130,* 32, 10456–10457.

WANG, Y., LIN, X., KIM, Y., CHANG, N., AND PEDTRAM, M. Enhancing efficiency and robustness of a photovoltaic power system under partial shading. *ISQED, 2012*, 592–600.

XIAO, W., OZOG, N., AND DUNFORD, W. 2007. Topology study of photovoltaic interface for maximum power point tracking. *Industrial Electronics, IEEE Transactions on 54,* 3, 1696 –1704.

YEOM, J., MOZSGAI, G., FLACHSBART, B., CHOBAN, E., ASTHANA, A., SHANNON, M., AND KENIS, P. 2005. Microfabrication and characterization of a silicon-based millimeter scale, pem fuel cell operating with hydrogen, methanol, or formic acid. *Sensors and Actuators B: Chemical 107,* 2, 882 – 891.

YUAN, L. AND QU, G. Dec. 2005. Analysis of energy reduction on dynamic voltage scaling-enabled systems. *IEEE Trans on CAD 24*, 1827–1837.

YUHUA, Z. AND LONGHUA, Q. 2009. A dynamic frequency scaling solution to dpm in embedded linux systems. *IEEE trans on Information Reuse & Integration*, 256–261.

ZHANG, Y. AND ETC. 2009. Small-signal modeling and analysis of battery-supercapacitor hybrid energy storage systems. *PES 09, IEEE*, 1–8.

ZHUO, J. AND CHAKRABARTI, C. 2009. Maximizing the lifetime of embedded systems powered by fuel cell-battery hybrids. *IEEE Trans. VLSI Syst 17*, 22–32.

ZHUO, J., CHAKRABARTI, C., CHANG, N., AND VRUDHULA, S. 2006. Extending the lifetime of fuel cell based hybrid systems. *DAC 2006 43rd ACM/IEEE*, 562–567.